

# Measurement of the electron density in Transient Spark discharge

Mário Janda, Viktor Martišovič, Karol Hensel, Lukáš Dvonč  
and Zdenko Machala

Division of Environmental Physics, Faculty of Mathematics, Physics and Informatics, Comenius University, Mlynska dolina F2, 84248 Bratislava, Slovakia

E-mail: [janda@fmph.uniba.sk](mailto:janda@fmph.uniba.sk)

Received 7 May 2014, revised 30 June 2014

Accepted for publication 29 July 2014

Published 4 September 2014

## Abstract

This paper presents our measurements of the electron density in a streamer-to-spark transition discharge, which is named transient spark (TS), in atmospheric pressure air. Despite the dc applied voltage, TS has a pulsed character with short ( $\sim 10$ – $100$  ns) high current ( $> 1$  A) pulses, with a repetition frequency on the order of kHz. The electron density  $n_e \sim 10^{17}$  cm $^{-3}$  at maximum is reached in TS with repetition frequencies below  $\sim 3$  kHz, using relatively low power delivered to the plasma (0.2–3 W).

The temporal evolution of  $n_e$  was estimated from the resistance of the plasma discharge, which was obtained by a detailed analysis of the electric circuit representing the TS and the discharge diameter measurements using a fast intensified charge-coupled device (iCCD) camera. This estimate was compared with  $n_e$  calculated from the measured Stark broadening of several atomic lines: H $_{\alpha}$ , N at 746 nm, and O triplet at 777 nm. Good agreement was obtained, although the method based on the plasma resistance is sensitive to an accurate determination of the discharge diameter. We have found that this method is also limited for strongly ionized plasmas. On the other hand, a lower  $n_e$  detection limit can be obtained by this method than from the Stark broadening of atomic lines.

Keywords: electron density, plasma resistance, Stark broadening, transient spark, self-pulsing discharge

(Some figures may appear in colour only in the online journal)

## 1. Introduction

Non-thermal plasma generated by electrical discharges can initiate chemical reactions in normally inert gaseous mixtures. The crucial parameter for the assessment of the plasma reactivity is the electron density  $n_e$ , since the whole non-thermal plasma chemistry is initially induced by the high energy electrons. Various experimental techniques have been used for the electron density measurement in plasmas. Commonly used laser spectroscopic methods are based on interferometry [1–3] and Thomson scattering [4]. Optical emission spectroscopy (OES) can also be used. A review of this topic was recently written by Ivkovic *et al* [5]. The most common OES method for the  $n_e$  measurement is based on the Stark broadening of atomic emission lines. The Stark broadening of tens of lines of various species have already

been studied (see [6, 7] and the references therein). The current can be state-of-the-art in Stark broadening theory as a theoretical basis for diagnostics of low temperature plasmas in gas discharges has recently been given by Stehlé *et al* [8].

Hydrogen-like and helium-like lines are the most sensitive to Stark broadening and they are the most commonly used for the determination of electron density in the plasma. The non-hydrogen lines of heavier neutral atoms are less sensitive to the Stark broadening, so they cannot be used for such low electron densities as hydrogen ones. At low  $n_e$ , the Stark broadening is also limited by other types of spectral lines broadening (instrumental, Doppler, Van der Waals). Except for the instrumental broadening, there are a variety of influences on the final line broadening in different types of plasma [9]. Recently, Palomares *et al* [10] showed that if the line fitting procedure is used to separate the effects of the different

broadening mechanisms, then the Stark broadening can be used, even below its theoretical validity regime. This was validated by Thomson scattering measurements, and the results show the agreement within 20% [10].

At high electron densities, the use of the  $H_\beta$  spectral line for the determination of the electron density is limited to  $n_e$  less than  $6 \times 10^{17} \text{ cm}^{-3}$  due to the strong Stark broadening and spectral proximity of other Balmer series lines such as  $H_\delta$  [11]. The  $H_\alpha$  line enables measurements of the electron densities of up to  $10^{19} \text{ cm}^{-3}$  for otherwise identical plasma conditions because it is typically by a factor of 4 narrower than the  $H_\beta$  line [11]. However, there is a fairly quantitative agreement between measured and calculated widths, shifts, and profiles but only for  $n_e$  below approximately  $10^{18} \text{ cm}^{-3}$ , serious disagreements were found beyond  $n_e \approx 10^{19} \text{ cm}^{-3}$  [12].

The use of lines of heavier atoms is the only alternative when hydrogen is not present, or at high electron temperatures where hydrogen is fully ionized [5]. The most intense atomic lines in the atmospheric pressure air plasmas are typically the lines of atomic oxygen and nitrogen. The broadening of the N atomic line at 746 nm was also recently used to diagnose a nanosecond repetitively pulsed (NRP) discharge [13]. The quadratic Stark effect of N given by Griem [14], with the correction introduced by Konjević [15] was used to do this. The whole procedure, including the handling of Van der Waals and instrumental broadening, was also described in [13] for an electron temperature of  $T_e = 10\,000 \text{ K}$ .

The difficulty with the Stark broadening is that it depends not only on  $n_e$  but also on electron temperature  $T_e$  and ion dynamics. This is not the case for the  $H_\beta$  line, where the dependence of Stark broadening on  $T_e$  is very weak. It is also relatively insensitive to ion dynamics, except for the line center dip [8]. This is the reason why  $H_\beta$  is frequently preferred over the  $H_\alpha$  line for the  $n_e$  calculation, even if the intensity of the  $H_\alpha$  line is much stronger, and it is usable for higher electron densities. The calculation of  $n_e$  from the full width at the half maximum (FWHM) of  $H_\alpha$  line is difficult due to the sensitivity to electron temperature and ion dynamics. However, Gigosos *et al* [16] showed that it is possible to avoid these difficulties using the full width at the half area (FWHA) instead of FWHM. Their calculations cover the range of electron densities between  $10^{14}$  and  $10^{19} \text{ cm}^{-3}$  and of electron temperatures between 1000 and 175 000 K. The emitter and the perturber ion kinetic temperature may vary within the interval  $(0.1-1) \times T_e$ .

The Stark broadening of the N atomic line near 746 nm also depends on the electron temperature. The proper use of this line for the determination of electron density is, therefore, possible only if we know  $T_e$ . On the other hand, the dependence of the Stark broadening of the atomic O triplet line near 777 nm on  $T_e$  is very weak. Another advantage of using the atomic O triplet line is the intensity of its emission. Actually, this triplet line is the strongest atomic line that we observe in atmospheric pressure air plasma generated by the transient spark (TS) discharge studied in this paper [17]. The disadvantage is that the three individual lines in this triplet interfere with each other due to the strong Stark effect. It would be necessary to use a complicated fitting procedure to separate these lines.

There is an alternative method for the calculation of  $n_e$ , which is derived from the conductivity and dimensions

of the plasma. Recently, this method was successfully used for calculation of  $n_e$  in NRP discharge [18], and also for the conductivity measurements of femtosecond laser-plasma filaments [19]. We used this approach for the calculation of time evolution of  $n_e$  in the TS discharge [20, 21]. The plasma conductivity was calculated using oscilloscopic measurements, while the plasma dimensions were obtained by time-resolved imaging using a high-speed iCCD camera. In previous study [21], we have already compared the electron density estimated from the plasma conductivity and calculated from FWHA of the Stark broadened  $H_\alpha$  line. In this paper, we compare the electron density estimated from the plasma conductivity with  $n_e$  calculated from the Stark broadening of  $H_\alpha$  line, N line at 746 nm, and O triplet line near 777 nm. Besides the FWHA, we used also FWHM of the  $H_\alpha$  line to calculate  $n_e$ . Reasonable agreement was obtained for  $T_e = 10\,000 \text{ K}$ . This electron temperature was also used to calculate  $n_e$  from the FWHM of the N line. Concerning the O triplet line, instead of using a fitting procedure for the separation of three individual lines, we tested the possibility of deriving  $n_e$  by comparing experimental and simulated spectra generated by Specpair software [9, 22].

### 1.1. Transient spark

Thanks to their high reactivity, atmospheric pressure plasmas have been tested for many potential applications, including bio-decontamination, surface processing, exhaust gas cleaning, and plasma assisted combustion [23–28]. The broad span of possible applications with different demands on the plasma characteristics implies that there is a large number of electrical discharges being used for the plasma generation. Besides established types of discharges, such as streamer corona [29] or dielectric barrier discharge (DBD) [30–32], new types of discharges or new types of reactors are still being developed and studied [33–35]. One of them is a DC driven self-pulsing discharge named TS [20, 36–39], which has already been successfully tested for several biological and environmental applications [40–42]. TS has been described relatively recently, but its concept is similar to the prevented spark studied by Marode *et al* in the late 1970s [43–45].

The TS is a filamentary streamer-to-spark transition discharge that is typically generated in a point-to-plane geometry with the electrode's gap  $\sim 0.5-1 \text{ cm}$  (see figure 1). The TS is initiated by a streamer (time  $\sim 0 \text{ ns}$  in figure 2), which transforms to a short ( $\sim 10-100 \text{ ns}$ ) spark current pulse (time  $\sim 100-200 \text{ ns}$  in figure 2). The streamer and the spark are two major phases of the TS discharge, responsible for two current pulses characteristic for the TS current waveforms (figure 2). Thanks to the short spark current pulse duration, the TS pulses generate highly reactive non-equilibrium plasma that can be maintained at relatively low energy conditions (up to 1 mJ/pulse) [20]. The short duration of the TS spark current phase results from the small amount of energy stored in the capacity  $C$  being discharged ( $\sim 10-40 \text{ pF}$ ).

The discharging capacity  $C$  is composed of several components (internal capacity of the discharge chamber  $C_{\text{int}}$ , capacity of the high voltage (HV) cable  $C_{\text{cable}}$  between the

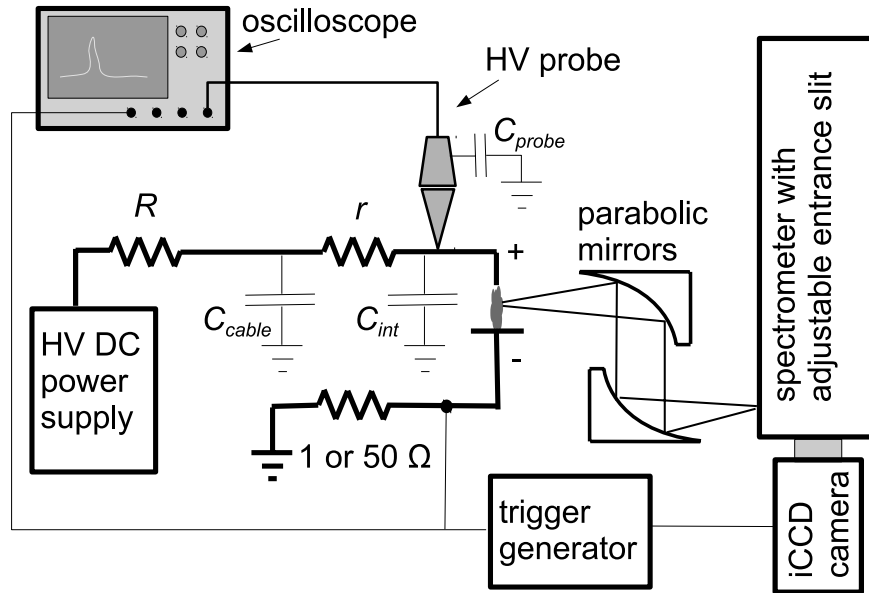


**Figure 1.** Simplified schematic of the experimental set-up generating the TS discharge.

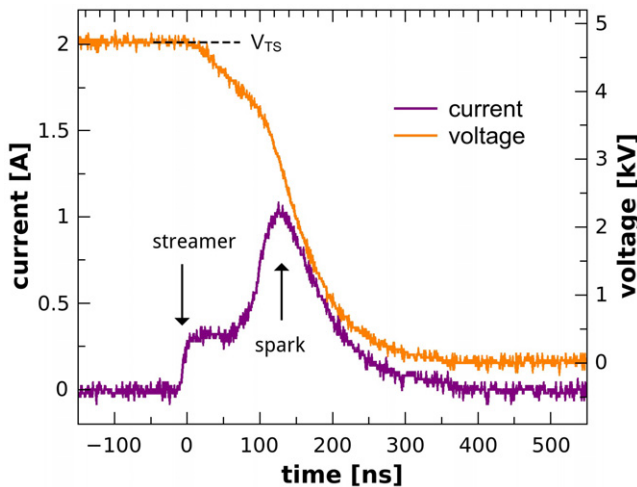


**Figure 2.** Typical waveforms of TS,  $f \approx 6$  kHz,  $C = 32 \pm 4$  pF,  $d = 5$  mm.

ballast resistor  $R$  and the electrode, and the capacity of the HV probe  $C_{HV} = 3$  pF). When  $C$  is discharged, the current, which is approximately given by

$$I(t) \approx -C \times \frac{dV(t)}{dt}, \quad (1)$$

reaches a high value ( $\sim 1$  A) and the voltage on the needle electrode drops to almost zero (figure 2). Then, during the quenched phase,  $C$  is recharged by a growing potential  $V$  on the stressed electrode. As soon as  $V$  reaches the characteristic TS breakdown voltage  $V_{TS}$ , a new TS pulse appears. TS generation is thus based on the charging and re-charging of capacity  $C$ . A characteristic repetition frequency  $f$  of this process is of the order of several kHz, and it can be controlled by the generator voltage  $V_g$ . The control of TS by  $V_g$  and other external circuit parameters was recently described in detail [20]. A more accurate version of equation (1), which takes into account the

influence of the ballast resistors  $R$  and  $r$ , was also provided therein.

Analysis of the electric circuit representing the TS described in [20] has enabled us to derive the plasma resistance  $R_p$  from the measured values of current and voltage waveforms. From  $R_p$ , we estimated the plasma conductivity  $\sigma_p$  using the equation:

$$\sigma_p = \frac{d}{R_p A} = \frac{4d}{\pi R_p D_p^2} \quad (2)$$

where  $d$  is the gap length,  $A$  and  $D_p$  are the cross-sectional area and diameter of the discharge channel, respectively. The electron density is related to the plasma conductivity  $\sigma_p$  by

$$n_e = \frac{\sigma_p m_e \nu_N}{e^2}. \quad (3)$$

Here  $e$  and  $m_e$  are the electron charge and mass, respectively, and  $\nu_N$  is the electron-heavy particles collision frequency.

Besides the voltage and current waveform, we thus need to know  $D_p$  and  $\nu_N$  to use this method to estimate  $n_e$ . In order to estimate  $D_p$ , we assumed that the discharge diameter can be well defined by the volume from which a light emission can be observed. We therefore performed a set of experiments of the TS imaging by iCCD camera. In the first approximation, we attributed the thickness of the illuminated area in the image to the plasma diameter. At low TS repetition frequencies (below 4 kHz), we observed shrinking of the discharge channel diameter during the streamer-to-spark transition from  $\sim 300 \mu\text{m}$  in the streamer phase, down to less than  $\sim 100 \mu\text{m}$  in the spark phase. This behavior is in agreement with the calculations of Naidis [46]. For the estimation of  $n_e$ , we used an average value  $200 \mu\text{m}$  for all phases of the TS discharge at all repetition frequencies.

In order to estimate  $\nu_N$ , we calculated  $\nu_N$  in air for the gas temperatures  $T_g$  from 300 to 3000 K, and for reduced electric field strengths  $E/N$  from 10 to 200 Td, using our package for Monte Carlo simulation of electron dynamics [47]. We found

that within this region of  $T_g$  and  $E/N$ , the value of  $\nu_N$  can vary from approximately from  $2 \times 10^{11}$  to  $4 \times 10^{12} \text{ s}^{-1}$ . We used a constant value  $10^{12} \text{ s}^{-1}$  for  $\nu_N$  during all phases of TS. This approximation introduces an uncertainty of less than a factor of 4.

The estimated electron density during the spark phase of TS with  $f < 4 \text{ kHz}$  was found to be  $\sim 10^{16} \text{ cm}^{-3}$  [20]. This is high enough to induce Stark broadening of atomic emission lines. We therefore verified it experimentally: first on the  $H_\alpha$  (656.28 nm) line, and next on the atomic lines of N (746 nm) and O (777 nm) to calculate  $n_e$  (section 3.1). We obtained good agreement between the electron densities calculated from these three different lines. Although we have used this measured  $n_e$  to verify the estimate of  $n_e$  from the plasma conductivity presented in our previous work [20], we found quite a significant disagreement. We therefore tried to find out how to improve the initial estimate of  $n_e$  presented in [20] (section 3.2). We mainly focused on the two major sources of the uncertainties in the estimate of  $n_e$  from the plasma conductivity, which are determination of the plasma diameter and the electron collision frequency. We performed additional TS imaging experiments with better analysis of the obtained images. With regard to the electron collision frequency, we tried to include the influence of the collisions with ions. Finally, we obtained much better agreement between the estimated and measured electron densities.

## 2. Experimental setup

Figure 1 shows a simplified schematic of the experimental set-up. Experiments were carried out at room temperature in atmospheric pressure air with a gas flow perpendicular to the discharge channel with a velocity of  $\sim 0.2 \text{ m s}^{-1}$ . A stainless-steel needle was used as a HV electrode opposite to a grounded planar copper electrode. The distance between electrodes  $d$  varied from 4 to 6 mm.

A DC HV power supply connected via a series resistor  $R$  limiting the total current was used to generate a positive TS discharge. The value of  $R$  varied from 3.5 to 9.84 M $\Omega$ . An additional small resistor  $r = 1 \text{ k}\Omega$  was attached directly to the HV electrode, separating it thus from a HV cable connecting it with the resistor  $R$  (figure 1). The purpose of adding  $r$  was to eliminate the oscillations of electric signals caused by internal inductances of the HV cable and of a grounding wire. The discharge voltage was measured by two 100 M $\Omega$  HV probes (Tektronix P6015A) at both ends of the resistor  $r$ . The currents at the grounded electrode were measured on a 50  $\Omega$  or 1  $\Omega$  resistor shunt. All of the current and HV signals were linked to the 200 MHz digitizing oscilloscope (Tektronix TDS2024) with a sampling rate of up to 2 Gs  $\text{s}^{-1}$ . For further analysis, the current and voltage signal time delay was corrected to take into account the different lengths of the BNC cables that we used.

Images of single TS pulses were taken by an intensified CCD camera (Andor Istar) with a time resolution down to 2 ns. The iCCD camera was triggered by a generator of 5 V rectangular pulses, which was triggered directly by the discharge current signal. The measurement of the discharge

current on the 50  $\Omega$  or 1  $\Omega$  resistor shunt enabled us to synchronize the acquisition of the emission, either with the beginning of the streamer (50  $\Omega$  shunt) or with the beginning of the spark (1  $\Omega$  shunt) phase of the TS. However, in both cases we were unable to acquire the initial 25 ns of the emission due to a delay caused by the trigger generator, the transmission time of the signal by BNC cables, and a camera insertion delay.

The time-resolved emission spectra were obtained using the same iCCD camera coupled to a 2 m monochromator (Carl Zeiss Jena PGS2) with resolving power 45 000, covering UV and VIS regions (200–800 nm). Here, the delay between the current signal and opening of the camera was compensated using a 10 m long optical cable (Ocean Optics P400-10-UV-VIS). The Gaussian FWHM of the instrumental broadening, measured by a He-Ne laser, changes between 0.04–0.09 nm for the entrance slit from 30  $\mu\text{m}$  to 100  $\mu\text{m}$ , respectively. Below 30  $\mu\text{m}$ , the entrance slit cannot improve the spectral resolution because it is limited by the size of the CCD chip pixels.

## 3. Results and discussion

### 3.1. Measurement of the electron density from Stark broadening of atomic lines

Since hydrogen atoms are the most sensitive to Stark broadening, we first focused on  $H_\alpha$  (656.28 nm) and  $H_\beta$  (486.13 nm) lines, despite the fact that the strongest atomic lines in the emission spectra in air are atomic lines of O and N [17]. To increase the intensity of H lines, the input ambient air was humidified by simply bubbling it through a vessel with water. Although we did not quantitatively measure the achieved humidity, it can be assumed to be a maximum of 3.17 kPa, based on the saturated vapor pressure and room temperature. The humidity was low enough to avoid significant changes of the TS properties. The emission spectra were measured with the gate time 20 ns, so the emission intensity of the observed hydrogen lines was quite weak. We, therefore, had to use  $H_\alpha$  line instead of the  $H_\beta$  line that was too weak, even though we accumulated a signal from up to 5000 pulses. Longer acquisition had no practical meaning due to random instabilities of the TS discharge.

In order to avoid problems with the dependence of the FWHM of the Stark broadened  $H_\alpha$  on  $T_e$ , we calculated  $n_e$  from the full width at the half area (FWHA) of the  $H_\alpha$  line using the formula derived by Gigosos *et al* [16]:

$$\Delta\lambda_{\text{FWHA}}^{H_\alpha} = 0.549 \text{ nm} \times \left( \frac{n_e}{10^{23} \text{ m}^{-3}} \right)^{0.67965} \quad (4)$$

Here,  $\Delta\lambda_{\text{FWHA}}^{H_\alpha}$  is the FWHA of the  $H_\alpha$  line in nm. In order to obtain reasonable values of  $n_e$ , the FWHA must be calculated from the line profile corrected with respect to Doppler, Van der Waals and instrumental broadening. However, the minimum value of FWHM that we experimentally measured was  $0.14 \pm 0.03 \text{ nm}$  (at time  $\sim 150 \text{ ns}$  after the peak of the spark current pulse,  $f \sim 2 \text{ kHz}$ ). These values are so large that Doppler broadening can be completely neglected. Even after the deconvolution of the measured line profile with the measured slit function describing our instrumental broadening,

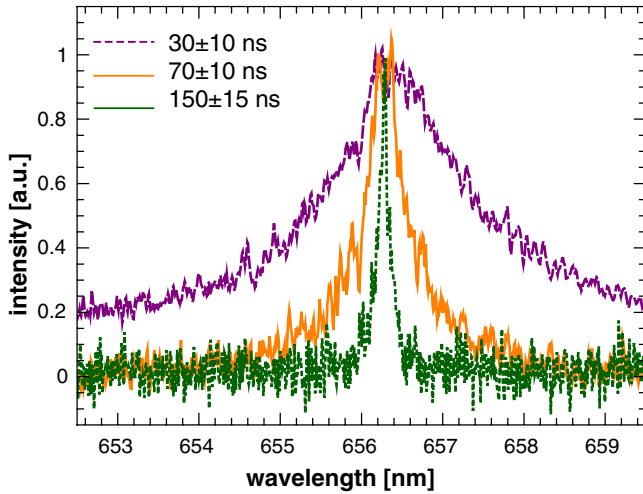


**Figure 3.** Normalized emission profiles of  $H_\alpha$  line at different times after the beginning of the spark phase of the TS,  $f \approx 2$  kHz.

the value of the FWHM (at 150 ns after the spark current pulse) stayed as high as  $\sim 0.12$  nm. Thus, the influence of instrumental broadening is within the experimental uncertainty of the measured value of FWHM.

The Van der Waals broadening  $\Delta\lambda_{\text{vdW}}$  can be calculated from the expression given by Djurović and Konjević [48]:

$$\Delta\lambda_{\text{vdW}} = 2.06 \times 10^{-13} \lambda_0^2 (\alpha \bar{R}^2)^{2/5} N \left( \frac{T_g}{\mu} \right)^{3/10}, \quad (5)$$

where  $\lambda_0$  is the wavelength at the center of the line,  $\alpha$  is the polarizability of the perturber,  $\mu$  is the reduced mass (kg),  $N$  is the neutral number density ( $\text{m}^{-3}$ ), and  $\bar{R}^2$  is the difference between the values of the square radius of the emitting atom in the upper and lower level. The necessary polarizabilities of the perturbers in air (nitrogen and oxygen) can be found in [49] and [50], respectively. At normal conditions, for  $H_\alpha$  line  $\Delta\lambda_{\text{vdW}} = 0.1$  nm. In the spark phase of the TS, the temperature is much higher ( $>2000$  K, see Annex 1) and the gas density is almost one order of magnitude lower than at normal conditions [46]. For these conditions, we estimated Van der Waals broadening to be less significant:  $\Delta\lambda_{\text{vdW}} \sim 0.02$  nm. This would decrease the measured  $H_\alpha$  line, broadening it to  $\sim 0.11$  nm (150 ns after the beginning of the spark phase), which is strictly due to the Stark broadening. In the spectra obtained closer to the beginning of the current peak, where the Stark broadening was even stronger, both the instrumental and Van der Waals broadening effects can be completely neglected. Figure 3 shows the time evolutions of the normalized  $H_\alpha$  line profiles.

The electron densities calculated from the Stark broadening of the  $H_\alpha$  line were so high ( $>10^{17} \text{ cm}^{-3}$ ) that even the atomic lines of N and O could be employed to calculate  $n_e$ , despite their weaker sensitivity to the Stark effect (figure 4, N line at 746 nm, figure 5, O triplet line at 777 nm). The advantage of using N or O atomic lines for the calculation of  $n_e$  from their Stark broadening is that they are present in dry air discharge. Moreover, the emission intensity is stronger and a better signal/noise ratio can be obtained without changing plasma properties by the additional humidity.

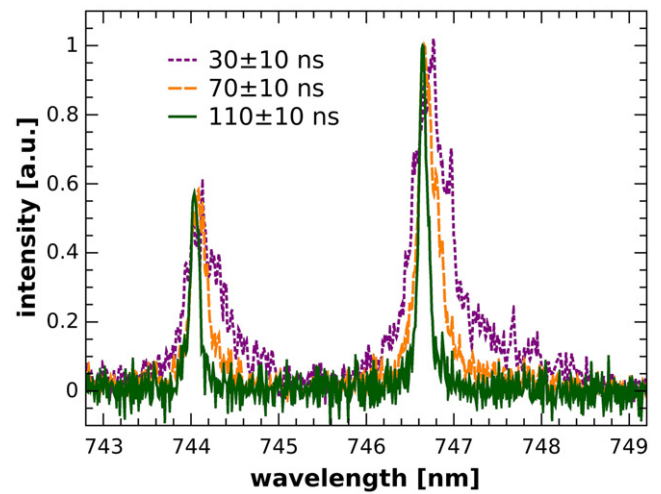


**Figure 4.** Normalized spectra of N around 746 nm in different times after the beginning of the spark phase of the TS,  $f \approx 1$  kHz.

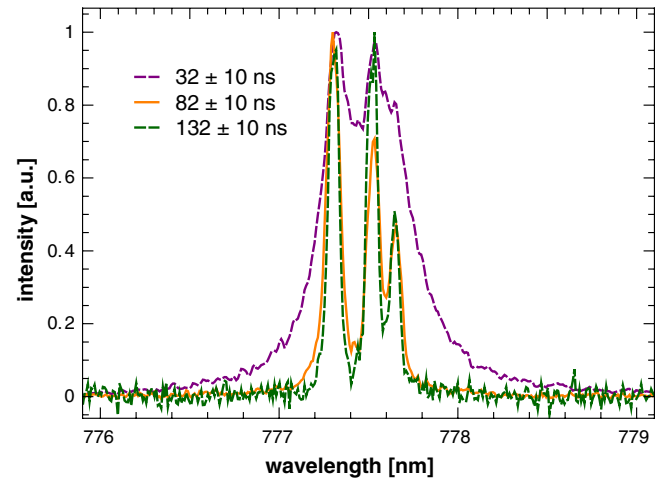


**Figure 5.** Normalized spectra of O triplet line around 777 nm in different times after the beginning of the spark phase of the TS,  $f \approx 1$  kHz.

The calculation of  $n_e$  from the N line (746 nm) Stark broadening in NRP discharge was recently presented [13]. The whole procedure, including the handling of Van der Waals and instrumental broadening, is well described therein. The quadratic Stark effect of N was given by Griem [14], the correction introduced by Konjević [15] was used. The Van der Waals broadening of the N line at 300 K and 1 atm was calculated to be 0.04 nm [13]. At our conditions, a much lower value was obtained:  $\Delta\lambda_{\text{vdW}} \sim 0.01$  nm. Besides the Stark broadening, the instrumental broadening is, therefore, the most important cause of the broadening of the measured lines. The pure Stark broadening width  $\Delta\lambda_{\text{Stark}}$  of the measured lines was obtained after deconvolution by the Gaussian instrumental broadening profile.

An additional error can be introduced by the uncertainty of  $T_e$  because the  $\Delta\lambda_{\text{Stark}}$  of N line depends on  $T_e$ . We could calculate  $T_e$  if we knew the reduced electric field strength  $E/N$  in the plasma channel. After the spark current pulse,  $E/N$  certainly decreases well below  $\sim 120$  Td, which is the breakdown  $E/N$  value, most probably to a value in the range

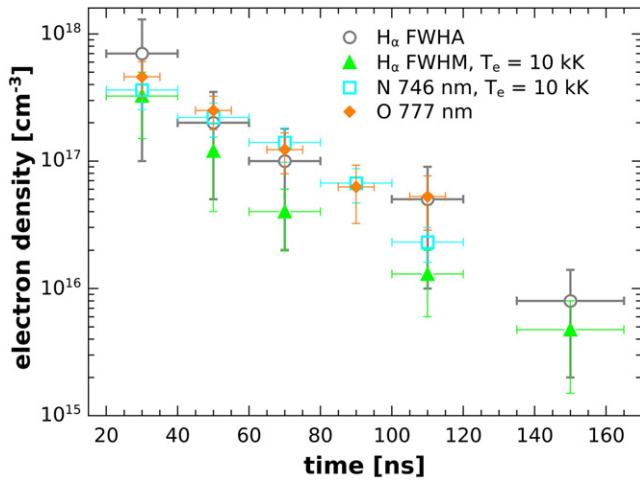


**Figure 6.** Comparison of electron density evolution after the beginning of the spark phase of the TS, calculated from the Stark broadening of  $H_\alpha$  line, N line at 746 nm and O triplet near 777 nm,  $f \sim 1\text{--}2\text{ kHz}$ .

from 10 Td to 70 Td. Fortunately, the dependence of  $T_e$  on  $E/N$  in air is weak in this range (see Annex 2). Moreover, the dependence of Stark broadening of the N line at 746 nm on  $T_e$  is also quite weak, in the range of  $T_e$  from 0.6 to 1.2 eV ( $\sim 5000\text{--}10\,000\text{ K}$ ) [51]. With a reasonable accuracy, we can assume  $T_e = 10\,000\text{ K}$ . We checked this assumption by calculating  $n_e$  from the FWHM of the  $H_\alpha$  line with  $T_e = 10\,000\text{ K}$  according to Vidal *et al* [52]. A fair agreement with  $n_e$  calculated from the FWHA of the  $H_\alpha$  line was obtained (figure 6). The electron density obtained from the Stark broadening of the N line at 746 nm is also in a good agreement with these data (figure 6) using  $T_e = 10\,000\text{ K}$ .

The dependence of Stark broadening of the O triplet ( $^5S^\circ, J = 2 \rightarrow ^5P, J = 1\text{--}3$ ) near 777 nm does not significantly depend on  $T_e$  and can be completely neglected. Another advantage of using this triplet to estimate  $n_e$  is that it is the strongest atomic line observed in VIS spectra of the TS discharge [17]. However, a disadvantage results from the overlapping of the three lines of the triplet at higher electron densities. The Stark broadening of this line is included in the Specair software package [9, 22]. We therefore used Specair to fit the experimental spectra to get  $n_e$  by changing the gas temperature, pressure, and the molar fraction of the electrons (figure 7). The advantage of using Specair is that simulated spectra can be convoluted with the measured instrumental broadening function. Doppler and Van der Waals broadenings are also included. Indeed, spectra have to be simulated under conditions relevant to experimentally measured spectra. The best results were obtained when we varied the molar fraction of electrons at  $T_g = 3000\text{ K}$  and a pressure of 1 atm. However, only small changes of estimated  $n_e$  were obtained for  $T_g$  from 1000 to 5000 K and pressures from 0.5 to 10 atm.

### 3.2. Estimation of the electron density from the plasma resistance

Values of  $n_e$  calculated from the measured  $H_\alpha$  line Stark broadening were compared with  $n_e$  estimated from the plasma

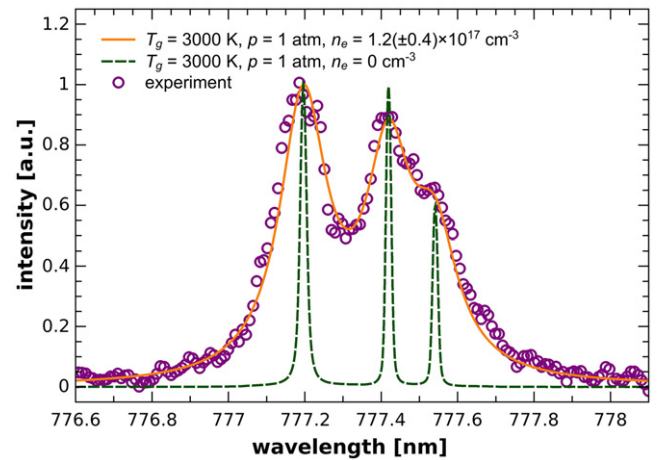


**Figure 7.** Experimental and Specair simulated spectra of O triplet emission line,  $f \approx 2\text{ kHz}$ ,  $\sim 70\text{ ns}$  after the rising slope of the spark pulse.

resistance calculation (formula (2) and (3)). It was found that the  $n_e$  measured from the Stark broadening is at least one order of magnitude higher than the initial estimate presented in [20]. The estimation of  $n_e$  from  $R_p$  brings forth some uncertainties from several sources. In addition to the uncertainty of  $R_p$  depending on the measured voltage and current, the discharge channel diameter  $D_p$ , and the collision frequency  $\nu_N$  are major sources of uncertainty in the estimation of  $n_e$  [20]. In the first step, we tested if the disagreement between the measured and estimated  $n_e$  can be resolved by more accurate estimates of the plasma diameter, which enters the cross-sectional area  $A$  of the plasma channel in formula (3) as a square.

For the estimation of  $n_e$ , we initially used an average value of the discharge diameter  $D_p = 200\ \mu\text{m}$  for all phases of the TS discharge. For a more accurate approximation of  $D_p$ , we performed additional time-resolved imaging of the TS discharge at different repetition frequencies. The aim was to obtain the time evolution of  $D_p$  during the evolution of the TS discharge. When we triggered the iCCD camera with a streamer current (measured on the  $50\ \Omega$  shunt) we imaged either the whole pulse (gate time  $0.5\text{--}2\ \mu\text{s}$ ) or the streamer only (gate time  $25\text{--}150\text{ ns}$ ). When we triggered with a spark current (measured on the  $1\ \Omega$  shunt) we imaged the spark phase only (gate time  $25\text{--}500\text{ ns}$ ). The beginning of the iCCD acquisition always started  $\sim 30\text{ ns}$  after the rising slope of the current signal due to the camera insertion delay and other delays in the circuit.

At low TS repetition frequencies (below 4 kHz) the streamer-to-spark transition phase is quite long, from a few hundred ns up to a few  $\mu\text{s}$  [37]. We therefore could not continuously follow the evolution of the discharge channel diameter from the beginning of the streamer until the end of the emission of the spark phase. In order to obtain  $D_p$ , we had to take an image of a single pulse. With a gate width of 25 ns we were able to determine  $D_p$  with a reasonable accuracy only for  $\sim 100\text{ ns}$  from the beginning of the streamer and for  $\sim 100\text{ ns}$  from the beginning of the spark phase. During these periods, we observed no significant changes in the  $D_p$ : neither after the streamer nor after the spark. On the other hand, we can compare the diameter of the discharge channel of the streamer

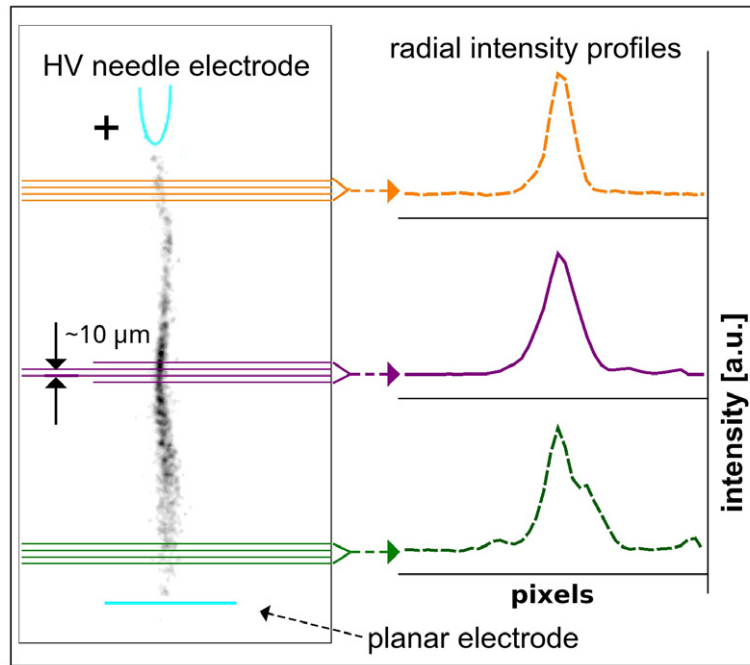


**Figure 8.** Image of a single TS pulse taken by an iCCD camera, 25 ns time resolution,  $f \approx 2$  kHz, spark phase, inverted colors. Radial intensity profiles at three different positions are shown for illustration.

and the spark phase. We can see a shrinking of the discharge channel diameter from  $\sim 300 \mu\text{m}$  in the streamer phase down to less than  $\sim 100 \mu\text{m}$  in the spark phase. These numbers represent the thickness of the illuminated area in the image of the plasma channel.

For a more accurate approximation of  $D_p$ , we used the FWHM of the spectrally unresolved radial intensity profile of the plasma channel. Instead of averaging over several pulses, we could improve the obtained radial emission profiles by summing the profiles from several rows on the iCCD chip (figure 8). After the Abel inversion, we found that the diameter of the streamer was  $\sim 150 \pm 40 \mu\text{m}$ . This agrees with the results of Gibert *et al* [53] or Van Veldhuizen *et al* [54], who also applied optical emission measurement.

The subsequent spark phase channel was found to be narrower (for  $f < 4$  kHz): less than  $100 \mu\text{m}$ . The FWHM of the radial emission profile of the spark phase after the Abel inversion is  $\sim 50 \pm 20 \mu\text{m}$ . Although it is slightly expanded near the planar electrode (see figures 8 and 9), we used the typical value for the region near the needle electrode, where we also measured the emission spectra of the  $H_\alpha$  line. Finally, the measured  $n_e$  from the Stark broadening of  $H_\alpha$  line agreed well with the estimate of  $n_e$  from the plasma resistance (figure 10), except for the first data point (30 ns after the beginning of the spark current pulse).

At higher TS frequencies ( $> 4$  kHz), the streamer-to-spark transition time in the TS decreases to only  $\sim 100$  ns [37] and we were able to observe the entire evolution of the discharge channel from the beginning of the streamer until the end of the spark. We found out that the contraction of the discharge channel during the spark phase was much weaker, or there was none. Therefore, at higher  $f$ , the approximation of  $D_p$  by a single value ( $\sim 150 \pm 40 \mu\text{m}$ ) is reasonable and a good agreement of the measured  $n_e$  from broadening of  $H_\alpha$  line with

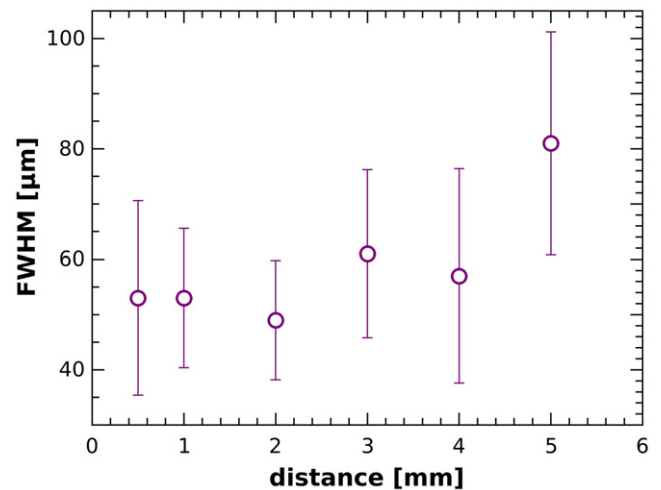


**Figure 9.** FWHM of the radial intensity profiles of single TS spark pulses as a function of the gap distance from the HV point electrode, after the Abel inversion,  $f \approx 2$  kHz.

the estimate of  $n_e$  from the plasma resistance was obtained using this approximation (figure 11).

For further improvement of the  $n_e$  estimation from the plasma resistance we focused on the collision frequency of the electrons. Based on  $H_\alpha$  line Stark broadening, the electron density during the TS spark current pulse is so high that the plasma is highly ionized. In order to obtain a better agreement between the estimated and measured  $n_e$  shortly after the spark current peak, it is necessary to include the collision of electrons with ions to calculate the overall collision frequency of electrons  $\nu_C$  [55]:

$$\nu_C = \nu_N + n_e v \sigma_{\text{Coul}}(n_e, T_e), \quad (6)$$

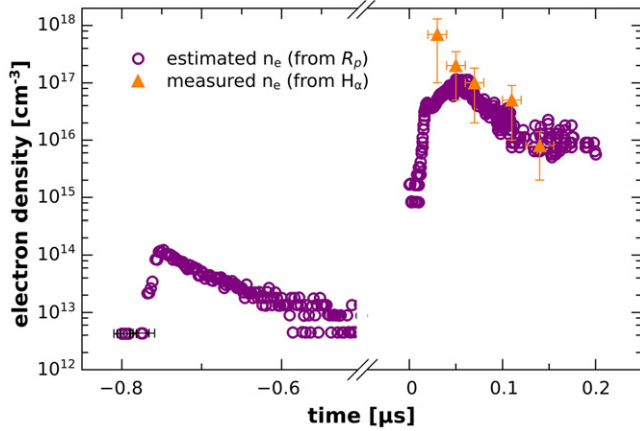


**Figure 10.** Electron density during the streamer and the spark phase of the TS pulse in  $\mu\text{s}$  time scale, estimated from the plasma resistance and measured by  $H_\alpha$  (FWHA) Stark broadening,  $f \approx 2$  kHz,  $C = 32 \pm 4$  pF, and  $d = 5$  mm.

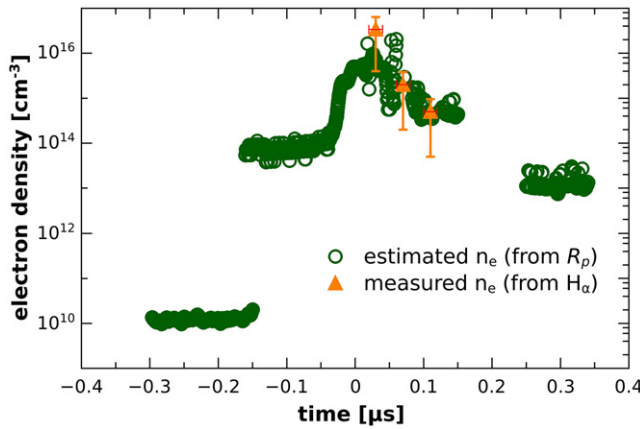


**Figure 11.** Electron density during the TS pulse, estimated from the plasma resistance and measured by  $H_\alpha$  (FWHA) Stark broadening,  $f \approx 6$  kHz,  $C = 32 \pm 4$  pF, and  $d = 5$  mm.

where  $v$  is the thermal velocity of electrons, and  $\sigma_{\text{Coul}}$  is the cross section of electron–ion collisions dominated by Coulomb forces. The expression for  $\sigma_{\text{Coul}}$  can be also found in [55]. The problem is that the  $v_C$  depends on both  $T_e$  and  $n_e$  in strongly ionized plasma, and the influence of  $T_e$  dominates. For this reason, the method of estimating  $n_e$  from  $R_p$  is not suitable for strongly ionized plasma. We can only say that the estimate of  $n_e$  from  $R_p$  is underestimated during the high current spark phase of TS.

In order to quantify the influence of electron–ion collisions, we calculated a correction factor that has to be used to multiply  $n_e$  calculated without the electron–ion collisions included. We expressed  $v_C$  as a function of electron–neutral collision frequency  $\nu_N$  ( $=10^{12} \text{ s}^{-1}$ ) and a correction factor  $\chi$  depending on the electron density and temperature:

$$v_C = \nu_N \times \chi(n_e, T_e), \quad (7)$$

The correction factor  $\chi$  increases with growing  $n_e$  and decreasing  $T_e$  (figure 12). The resulting error of  $n_e$  calculated using  $\nu_N$  must, therefore, be the highest right after the end of the spark pulse where  $n_e$  is still very high ( $>10^{17} \text{ cm}^{-3}$ ),

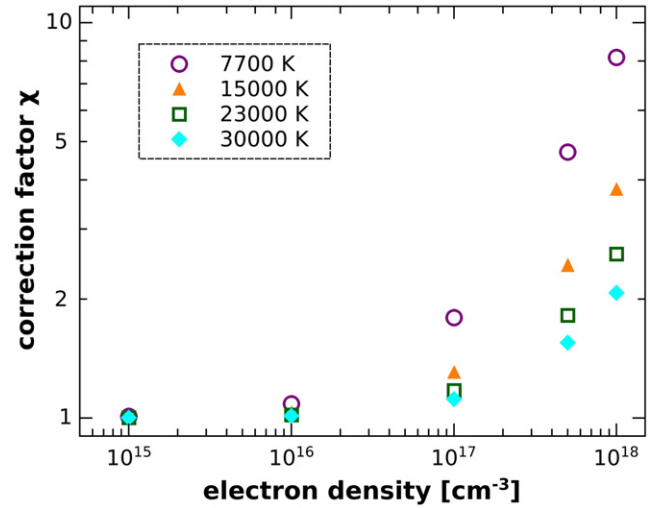


**Figure 12.** Correction factor for the calculation of electron collision frequency including electron–ion collisions, as a function of electron density and electron temperature.

but the electron temperature decreases to  $\sim 10\,000$  K. For  $n_e = 5 \times 10^{17} \text{ cm}^{-3}$  measured by the Stark broadening of  $H_\alpha$  line at  $f \approx 2$  kHz and  $T_e \approx 10\,000$  K, we get  $\chi \approx 4$ . If we apply this correction factor, we would get a better agreement between the estimated and measured  $n_e$  at 30 ns after the beginning of the spark current peak (figure 10). Later, both  $n_e$  and the influence of electron–ion collisions decreases, and the approximation based on  $\nu_N$  is valid again.

With increasing repetition frequency, the TS current pulses become smaller and broader [37]. The electron density of  $n_e$  in the spark phase, therefore, also decreases with the increasing  $f$ . The maximum  $n_e$  reaches  $\sim 10^{16} \text{ cm}^{-3}$  at  $f \approx 6$  kHz (figure 11). We assume that the ionization degree is low and the estimate of  $n_e$  from  $R_p$  is closer to the real value than at  $f < 4$  kHz, without the electron–ion collisions included.

However, the agreement between these two methods could be to some degree accidental. The diameter obtained from the spectrally unresolved emission need not necessarily be identical to the real ‘electrical’ plasma diameter. Moreover, the emission profiles from which  $D_p$  was derived were Abel inverted, while the atomic lines were obtained from the line-in-sight integrated emission. The line-in-sight integrated emission scan is dominated by emission from the central plasma core. Thus, the line-of-sight measurement provides, to a good approximation, the  $n_e$  at the centerline of the plasma [9]. As a result, the  $n_e$  from the Stark broadening should be higher than the  $n_e$  derived from the plasma conductivity. This could also partially explain the big discrepancy observed at lower TS frequencies shortly after the beginning of the spark phase of TS, although there are other possible explanations, as discussed in the next paragraphs.

The strong degree of ionization at the beginning of the spark phase of TS disqualifies not only the method based on  $\sigma_p$  but it can also influence  $n_e$  obtained from the Stark broadening of atomic lines. A proper subtraction of the continuum background is important to get the correct FWHM of these lines. We approximated the background subtracted

from these lines by linear functions. This could introduce some additional inaccuracy determining FWHM (or FWHA), particularly in the early time of the spark phase of the TS, where the  $H_\alpha$  line is significantly broadened and the linear approximation of the background continuum could be less accurate.

Finally, another source of uncertainty in  $n_e$ , as measured from the Stark effect, could be due to the space charge field  $F_c$ , especially at the beginning of the spark phase when the conductivity is still low. The  $F_c$  also induces the Stark effect and influences the line width [56] if  $F_c$  is not negligible compared to the microfields  $F_o$  from the ions surrounding excited H atoms, which is called Holtsmark field [57]. Reference [56] shows how the line profile may change with the parameter  $p_c = F_c/F_o$  and with the electron temperature  $T_e$ . Namely, a table is given for  $H_\alpha$  and  $n_e = 10^{17} \text{ cm}^{-3}$ .

At the beginning of the spark phase of TS at lower frequencies, the  $F_c$  can be as high as  $14 \text{ kV cm}^{-1}$  (breakdown voltage  $\sim 7 \text{ kV}$ , gap  $5 \text{ mm}$ ). The Holtsmark field  $F_o$  in  $\text{V cm}^{-1}$  is given by [57]:

$$F_o = 3.75 \times 10^{-7} n_i^{2/3}, \quad (8)$$

where  $n_i$  is the density of ions in  $\text{cm}^{-3}$ . If  $n_i \approx n_e = 10^{17} \text{ cm}^{-3}$ ,  $F_o \approx 80 \text{ kV cm}^{-1}$ , and the parameter  $p_c \approx 0.175$ . Referring to [56], it seems that the influence of  $F_c$  is minor but not negligible. This effect could thus slightly contribute to the overestimation of  $n_e$  obtained from the Stark broadening (e.g. 30 ns after the beginning of the spark current pulse, figure 10). However, 30 ns after the beginning of the spark current pulse, the conductivity is already much higher than at the beginning of the spark phase (current rising slope), the voltage drops to a low value and  $F_c$  will not be as high as  $14 \text{ kV cm}^{-1}$ . It is probably much lower and so probably negligible compared to  $F_o$ . This is certainly true in the later phase after the spark current pulse, which makes the  $n_e$  measured from the Stark broadening more realistic.

#### 4. Conclusions

TS, which is a DC-driven self-pulsing discharge, was investigated. TS represents a repetitive streamer-to-spark transition discharge of very short pulse duration ( $\sim 10\text{--}100 \text{ ns}$ ) with a very limited energy, so that the generated plasma stays out of equilibrium. This discharge can be maintained at low energy conditions (up to  $1 \text{ mJ/pulse}$ ) by an appropriate choice of the resistances and capacities in the electrical circuit. Its frequency can be controlled by the applied voltage. The chemical activity of the TS is comparable with the nanosecond repetitive pulsed discharges, its advantages include the ease of the DC operation and no need for special and expensive high voltage pulsers with high repetitive frequency and nanosecond rise-times. An electron density  $n_e$  as high as  $10^{17} \text{ cm}^{-3}$  in the spark phase of the TS at repetition frequency  $\sim 2 \text{ kHz}$  can be achieved.

We characterized the evolution of  $n_e$  in the TS discharge using two methods: the  $n_e$  was calculated from the plasma resistance and from the Stark broadening of atomic lines

measured by time resolved OES. Finally, good agreement between these two methods was obtained. However, an accurate estimate of the discharge channel diameter  $D_p$  is critical for the calculation of  $n_e$  from the plasma resistance. A fast iCCD camera was used for time-resolved imaging of the TS discharge to obtain  $D_p$ , which is defined as a full width at the half maximum of the radial intensity profile of the discharge channel after the Abel inversion. Different values of  $D_p$  had to be used for the streamer ( $\sim 150 \mu\text{m}$ ) and the spark ( $\sim 50 \mu\text{m}$ ) phases of the TS discharge at lower repetition frequencies ( $< 4 \text{ kHz}$ ) because the  $D_p$  has contracted in the spark phase. At higher frequencies, no discharge channel contraction occurred during the streamer-to-spark transition phase and a single value of  $D_p$  typical for the streamer could be used to calculate  $n_e$ .

The estimate of  $n_e$  from the plasma resistance is less sensitive to the collision frequency of electrons. With a reasonable accuracy, a single value  $10^{12} \text{ s}^{-1}$  can be used for a weakly ionized non-equilibrium air plasma for the gas temperature  $T_g$  from 300 to 3000 K and for the reduced electric field strength  $E/N$  from 10 to 200 Td. However, this method is not suitable for a strongly ionized plasma where collisions of electrons with charged particles cannot be neglected. This defines the upper limit of this method. In our case, we can use it only for  $n_e < 10^{17} \text{ cm}^{-3}$ . The lower detection limit of this method depends mostly on the accuracy of the current measurement, from which the plasma resistance is calculated. For the current measured on a  $50 \Omega$  shunt, our detection limit is  $10^{12}\text{--}10^{13} \text{ cm}^{-3}$ . This limit is lower than using Stark broadening of atomic lines.

The detection limit of the method based on the Stark broadening of atomic lines is given by several parameters. The Stark broadening must surpass other broadening mechanisms (instrumental, van der Waals, and Doppler), and it also depends on the intensity of the emission signal. The lowest electron density we have measured from the Stark broadening was slightly below  $10^{15} \text{ cm}^{-3}$ , using full width at the half area FWHA of the  $H_\alpha$  line. We could, therefore, calculate  $n_e$  from the Stark broadening of the atomic lines only during the spark phase of TS, while the plasma resistance method enabled us to also calculate  $n_e$  during the streamer phase. The advantage of the Stark broadening method is that it is also valid in strongly ionized plasma. The FWHA of the  $H_\alpha$  line can be theoretically used for  $n_e$  up to  $10^{19} \text{ cm}^{-3}$  [16].

We measured the Stark broadening of three different lines:  $H_\alpha$  line, N line at  $746 \text{ nm}$  and O triplet line at  $777 \text{ nm}$ . We obtained the same  $n_e$  from all of them within the experimental uncertainty. The use of each of these lines has a number of advantages and disadvantages. The  $H_\alpha$  line is the most sensitive to the Stark effect, it should also have the lowest detection limit for  $n_e$ . When using the FWHA of the  $H_\alpha$  line for the calculation of  $n_e$ , we avoid the dependence of the Stark effect on the electron temperature  $T_e$ . On the other hand, the intensity of the  $H_\alpha$  line in humid air plasma is typically much weaker than the intensity of N and O lines, it is not available at all in dry air.

The most suitable atomic lines for the calculation of  $n_e$  in dry air are atomic lines of N and O. The method is relatively straightforward for N line at  $746 \text{ nm}$  if  $T_e$  is known. We found

that, for the spark phase of TS shortly after the spark current pulse,  $T_e = 10\,000$  K can be used with a reasonable accuracy. The influence of  $T_e$  on the broadening of the O triplet line at 777 nm is weak and can be neglected. The disadvantage of using O triplet line results from the mutual overlapping of its three lines at higher electron densities. We showed that it is possible to use Specair software [9, 22] to fit the experimental spectra to get  $n_e$  from this triplet line. The advantage of using Specair is that simulated spectra can be convoluted with the measured instrumental broadening function. Doppler and Van der Waals broadenings can also be included.

The measured evolution of  $n_e$  during different phases of the TS discharge is useful for its better understanding and easier adaptation for specific applications. It also helps us to assess the reactivity of the plasma generated by the TS. The decrease of maximum  $n_e$  with the increasing TS repetition frequency can be explained by the decrease of the reactivity of generated plasma. However, it is necessary to perform kinetic modeling of TS in air to confirm this assumption. For this purpose, we are developing a kinetic model of TS based on ZDPlasKin package [58]. The goal is to mimic the evolution of the reduced electric field strength  $E/N$  during all phases of TS, so that the calculated electron densities agree with experimental data presented in this paper. Once this goal is fulfilled, a validated kinetic model of TS will help us to further understand the induced plasma chemistry.

## Annexes

### Annex 1—Gas temperature measurement from $N_2$ emission spectra

We used the time-resolved spectra of the  $N_2$  2<sup>nd</sup> ( $C^3\Pi_u - B^3\Pi_g$ ) positive system to determine the gas temperature  $T_g$ , assuming that it approximately equals the rotational temperature of excited  $N_2(C^3\Pi_u)$  species. This rotational temperature was inferred from the spectra using SPECAIR package [9, 22]. The ICCD camera was synchronized with the beginning of the spark pulse—by the current signal measured on 1  $\Omega$  shunt.

Previously we measured changes of the temperature at the beginning of the streamer and a subsequent evolution of the temperature during the streamer-to-spark transition phase [37]. The steady-state gas temperature, measured at the beginning of the streamers initiating the TS, increased from an initial value of  $\sim 300$  K only up to  $\sim 550$  K at repetition frequency 10 kHz. After the streamer, an increase of the temperature increased up to  $\sim 1000$  K, as measured at the beginning of the spark phase. A further increase of the gas temperature up to  $\sim 2500$  K was observed at  $f \approx 6$  kHz.

For the purposes of the study presented in this paper, we focused on the gas temperature in the spark phase of TS at various repetition frequencies. Figure 13 shows the highest temperature derived from the time-resolved spectra of the  $N_2$  2<sup>nd</sup> ( $C^3\Pi_u - B^3\Pi_g$ ) positive system as a function of  $f$ , with time resolution 20 ns. The uncertainty in these data is quite high at lower TS repetition frequencies, despite the accumulation over 1000 pulses. The  $N_2(C^3\Pi_u)$  species

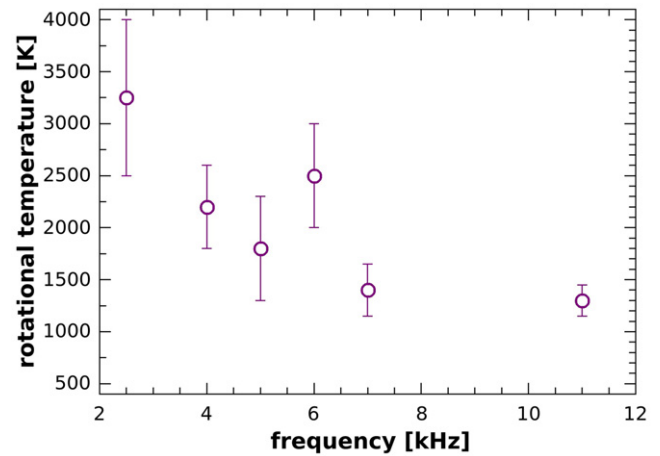


**Figure 13.** The highest temperature during the spark phase of TS, approximated by the rotational temperature derived from the time-resolved spectra of the  $N_2$  2<sup>nd</sup> positive system ( $C^3\Pi_u - B^3\Pi_g$ ) as a function of  $f$ , with time resolution 20 ns.

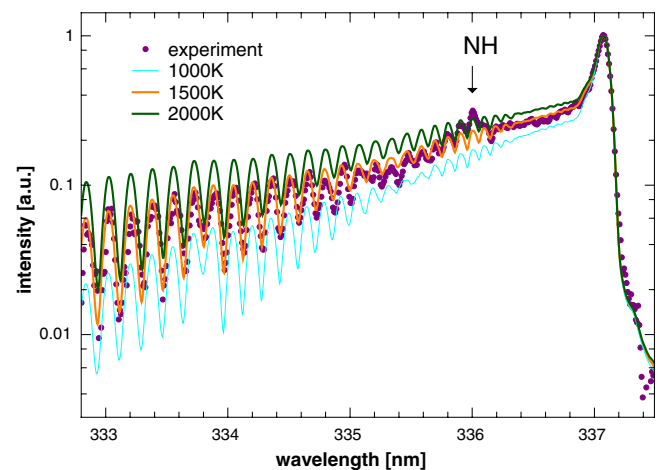


**Figure 14.** Experimental and Specair simulated spectra of 0-0 transition of  $N_2$  2<sup>nd</sup> positive system,  $f \approx 2$  kHz,  $\sim 30$  ns after the beginning of the spark pulse (not the spectrum from which the highest temperature at  $f \approx 2$  kHz was determined).

are produced mainly during the streamer phase of the TS discharge [37] and their life time is so short that they decay before the onset of the spark phase of the TS at lower repetition frequencies. At  $f > 3$  kHz, with much shorter streamer-to-spark transition phase, during the spark phase, we still observed quite a strong emission from  $N_2(C^3\Pi_u)$  generated during the streamer. At lower TS frequencies, we depend on a small amount of  $N_2(C^3\Pi_u)$  species that are generated during the spark phase. Moreover, there is interference of the NH emission with the strongest emission band of the  $N_2(C^3\Pi_u)$  species (0-0 vibrational transition, figure 14). The use of other vibrational transition bands does not significantly improve the uncertainty of the calculated temperature, which is due to a weaker signal.

### Annex 2—Monte Carlo simulations of electron dynamics

The calculation of the mean electron energy and their temperature  $T_e$  requires a knowledge of the electron

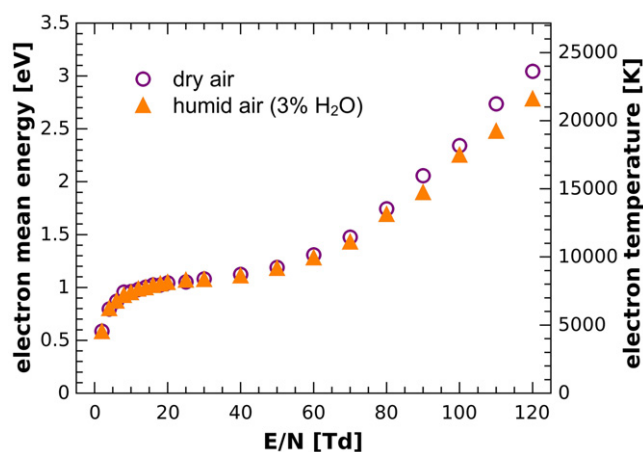


**Figure 15.** Electron mean energy and electron temperature in dry and humid air (3% H<sub>2</sub>O) as functions of the reduced electric field strength  $E/N$ .

energy distribution function (EEDF). In non-equilibrium cold plasmas, EEDFs may have strongly non-Maxwellian shapes, but they satisfy the Boltzmann equation. Thus, one way to obtain EEDFs is to solve simplified versions of the Boltzmann equation numerically. The second approach is to use Monte Carlo (MC) methods. We use an open source software program named ‘Web-EEDF’ for the calculation of EEDF [47, 59, 60], which is based on the algorithm presented by Tas *et al* [61]. ‘Web-EEDF’ derives the EEDF from the MC simulation of electron dynamics in constant electric fields in gas mixtures. The reliability of ‘Web-EEDF’ was checked by comparison with the data found in literature [59, 60].

Besides the composition of the gas, the major factor determining the EEDF is the reduced electric field strength ( $E/N$ ). The problem is that we do not really know the value of  $E/N$  in the plasma channel generated by the TS discharge. However, after the spark current pulse,  $E/N$  certainly decreases well below  $\sim 120$  Td, which is the breakdown  $E/N$  value, most probably to a value in the range from 10 Td to 70 Td. Fortunately, the dependence of  $T_e$  on  $E/N$  in both humid and dry air is weak in this range (figure 15). With a reasonable accuracy, we therefore assumed that  $T_e = 10\,000$  K during the period shortly after the spark pulse of the TS discharge.

## Acknowledgments

This work was sponsored by the Slovak Research and Development Agency APVV-0134-12, and Slovak grant agency VEGA 1/0998/12.

## References

- [1] Walkup R E, Jasinski J M and Dreyfus R W 1986 *Appl. Phys. Lett.* **48** 1690
- [2] Doyle L A 1999 *IEEE Trans. Plasma Sci.* **27** 128
- [3] Villagran M, Sobral H and Camps E 2001 *IEEE Trans. Plasma Sci.* **29** 613
- [4] Sheffield J, Froula D, Glenzer S H and Luhmann N C Jr 2010 *Plasma Scattering of Electromagnetic Radiation* 2nd edn (Amsterdam: Elsevier)
- [5] Ivkovic M, Jovicevic S and Konjevic N 2004 *Spectrochim. Acta B* **59** 591
- [6] Konjevic N *et al* 2002 *J. Phys. Chem. Ref. Data* **31** 819
- [7] Lesage A 2009 *New Astron. Rev.* **52** 471
- [8] Stehlé C, Busquet M, Gilles D and Demura A V 2005 *Laser Particle Beams* **23** 357
- [9] Laux C O, Spence T G, Kruger C H and Zare R N 2003 *Plasma Sources Sci. Technol.* **12** 125
- [10] Palomares J M *et al* 2012 *Spectrochim. Acta B* **73** 39
- [11] Parigger C G and Oks E 2010 *Int. Rev. At. Mol. Phys.* **1** 13
- [12] Griem H R 2000 *Contrib. Plasma Phys.* **40** 46
- [13] van der Horst R M *et al* 2012 *J. Phys. D: Appl. Phys.* **45** 345201
- [14] Griem H R 1964 *Plasma Spectrosc.* (New York: McGraw-Hill)
- [15] Konjević N 1999 *Phys. Rep.* **316** 339
- [16] Gigos M, Gonzalez M and Cardenaso V 2003 *Spectrochim. Acta B* **58** 1489
- [17] Machala Z, Janda M, Hensel K, Jedlovský I, Leštinská L, Foltin V, Martišoviš V and Morvová M 2007 *J. Mol. Spectrosc.* **243** 194
- [18] Pai D Z, Lacoste D A and Laux C O 2010 *Plasma Sources Sci. Technol.* **19** 065015
- [19] Fischer R P, Ting A C, Gordon D F, Ferrisler R F, DiComo G P and Sprangle P 2007 *IEEE Trans. Plasma Sci.* **35** 1430–6
- [20] Janda M, Martišoviš V and Machala Z 2011 *Plasma Sources Sci. Technol.* **20** 035015
- [21] Machala Z, Pai D Z, Janda M and Laux C O 2013 Atmospheric pressure nanosecond pulsed discharge plasmas *Low Temperature Plasma Technology: Methods and Applications* (Boca Raton: CRC Press)
- [22] Laux C O 2002 *Radiation and Nonequilibrium Collisional-Radiative Models (Lecture Series 2002–07, Physico-Chemical Modeling of High Enthalpy and Plasma Flows)* (Rhode-Saint-Genèse, Belgium: von Karman Institute)
- [23] Penetrante B and Schultheis S E (ed) 1993 *Non-Thermal Plasma Techniques for Pollution Control (NATO ASI series Part A)* (Berlin: Springer)
- [24] Inagaki N (ed) 1996 *Plasma Surface Modification, Plasma Polymerization* (Lancaster: Technomic)
- [25] Fridman A 2008 *Plasma Chemistry* (New York: Cambridge University Press)
- [26] Starikovskaia S M and Starikovskii A Y 2010 Plasma assisted ignition, combustion *Handbook on Combustion* vol 1 Fundamentals, Safety (Weinheim: VCH Wiley)
- [27] Machala Z, Hensel K and Akishev Y (ed) 2012 *Plasma for Bio-decontamination, Medicine, Food Security (NATO Science for Peace, Security Series A—Chemistry, Biology)* (Heidelberg: Springer)
- [28] Parvulescu V I, Magureanu M and Lukeš P (ed) 2013 *Plasma Chemistry, Catalysis in Gases, Liquids* (Weinheim, Germany: Wiley)
- [29] Loeb L B 1965 *Electrical Coronas* (Berkeley: University of California Press)
- [30] Efremov N M, Adamiak B Y, Blochin V I, Dadashev S J, Dmitriev K I, Gryaznova O P and Jusbashev V F 2000 *IEEE Trans. Plasma Sci.* **28** 238
- [31] Wagner E, Brandenburg R, Kozlov K V, Sonnenfeld A, Michel P and Behnke J F 2003 *Vacuum* **71** 417
- [32] Kogelschatz U 2003 *Plasma Chem. Plasma Process.* **23** 1
- [33] Cernak M, Rahel J, Kovacic D, Simor M, Brablec A and Slavicek P 2004 *Contrib. Plasma Phys.* **44** 492
- [34] Becker K H, Kogelschatz U, Schoenbach K H and Barker R J (ed) 2005 *Non-equilibrium Air Plasmas at Atmospheric Pressure* (Bristol: IOP Publishing)
- [35] Pai D, Lacoste D A and Laux C O 2008 *IEEE Trans. Plasma Sci.* **36** 974–5
- [36] Machala Z, Jedlovský I and Martišoviš V 2008 *IEEE Trans. Plasma Sci.* **36** 918–9

- [37] Janda M, Machala Z, Niklová A and Martišovits V 2012 *Plasma Sources Sci. Technol.* **21** 045006
- [38] Gerling T, Hoder T, Brandenburg R, Bussiahn R and Weltmann K-D 2013 Simulation of streamer- induced pulsed discharges in atmospheric-pressure air *J. Phys. D: Appl. Phys.* **46** 145205
- [39] Gerling T, Hoder T, Bussiahn R, Brandenburg R and Weltmann K-D 2013 Simulation of streamer- induced pulsed discharges in atmospheric-pressure air *Plasma Sources Sci. Technol.* **22** 065012
- [40] Machala Z, Morvová M, Marode E and Morva I 2000 *J. Phys. D: Appl. Phys.* **33** 3198
- [41] Machala Z, Jedlovský I, Chládeková L, Pongráč B, Giertl D, Janda M, Šikurová L and Polčič P 2009 *Eur. Phys. J. D* **54** 195
- [42] Janda M, Machala Z, Lacoste D A, Stancu G D and Laux C O 2012 Stabilization of a lean methane-air flame using transient spark discharge *13th Int. Symp. on High Pressure Low Temperature Plasma Chemistry (Hakone XIII) (Kazimierz Dolny, Poland, 9–14 September)* pp 185–9
- [43] Bastien F and Marode E 1979 *J. Phys. D: Appl. Phys.* **12** 249
- [44] Marode E, Goldman A and Goldman M 1993 High pressure discharge as a trigger for pollution control *Non-Thermal Plasma Techniques for Pollution Control ( NATO ASI series, Part A)* pp 167–90 (Berlin: Springer)
- [45] Hafez R, Samson S and Marode E 1995 A prevented spark reactor for pollutant control. Investigation of NO<sub>x</sub> removal *Proc. 12th Int. Symp. on Plasma Chemistry (ISPC) (Minneapolis, USA)* vol 2 pp 855–61
- [46] Naidis G V 2009 *Eur. Phys. J. Appl. Phys.* **47** 22803
- [47] Janda M, Martišovits V, Morvová M, Machala Z and Hensel K 2007 *Eur. Phys. J. D* **45** 309
- [48] Djurović S and Konjević N 2009 *Plasma Sources Sci. Technol.* **18** 035011
- [49] Bates D R and Bederson B (ed) 1985 *Advances in Atomic, Molecular Physics* vol 20 (New York: Academic)
- [50] Nir S, Adams S and Rein R 1973 *J. Chem. Phys.* **59** 3341
- [51] Plavčan J, Grolmusova Z, Rakovsky J, Čermak P and Veis P 2010 Determination of Stark broadening parameters for O, N from H<sub>α</sub> using laser induced breakdown spectroscopy *Proc. 19th Annual Conf. of Doctoral Students (Prague, Czech Republic)* pp 101–4
- [52] Vidal C R, Cooper J and Smith E W 1973 *Astrophys. J. Suppl. Ser.* **25** 37–136
- [53] Gibert A and Bastien F 1989 *J. Phys. D: Appl. Phys.* **22** 1078–82
- [54] van Veldhuizen E M, Kemps P C M and Rutgers W R 2002 *IEEE Trans. Plasma. Sci.* **30** 162
- [55] Raizer Yu P 1991 *Gas Discharge Physics* (Berlin: Springer)
- [56] Bastien F and Marode E 1977 *J. Quant. Spectrosc. Radiat.* **17** 453
- [57] Kunze H-J 2009 *Introduction to Plasma Spectroscopy* (Berlin: Springer)
- [58] Pancheshnyi S, Eismann B, Hagelaar G J M and Pitchford L C 2008 Computer code zdp1skin <http://www.zdp1skin.laplace.univ-tlse.fr> (University of Toulouse, LAPLACE, CNRS-UPS-INP, Toulouse, France)
- [59] Janda M, Machala Z, Morvova M, Francek V and Lukac P 2005 *Acta Phys. Slov.* **55** 507
- [60] Janda M, Hensel K, Martišovits V and Morvova M 2006 *Czech. J. Phys.* **56** B774
- [61] Tas M A, van Veldhuizen E M and Rutgers W R 1997 *J. Phys. D: Appl. Phys.* **30** 1636